Pressure-dependent elastic constants and sound velocities of wurtzite SiC, GaN, InN, ZnO, and CdSe, and their relation to the high-pressure phase transition: A first-principles study

Kanoknan Sarasamak
College of KMITL Nanotechnology, King Mongkut's Institute of Technology Ladkrabang, Bangkok 10520, Thailand

Sukit Limpijumnong
School of Physics, Suranaree University of Technology and Synchrotron Light Research Institute, Nakhon Ratchasima 30000, Thailand and Thailand Center of Excellence in Physics (ThEP Center), Commission on Higher Education, Bangkok 10400, Thailand

Walter R. L. Lambrecht
Department of Physics, Case Western Reserve University, Cleveland, Ohio 44106-7079, USA
(Received 12 March 2010; revised manuscript received 19 May 2010; published 1 July 2010)

Elastic constants and sound velocities calculated from first principles as function of pressure are presented for wurtzite SiC, GaN, InN, ZnO, and CdSe. The C_{11} and C_{33} elastic constants, which are involved in longitudinal sound waves along symmetry directions, are found to monotonically increase with pressure. The shear moduli C_{44} and C_{66}, which are involved in transverse sound waves along symmetry directions, either decrease with increasing pressure or initially increase from zero pressure but then turn over and start decreasing. Of special interest is the pressure at which the C_{44} and C_{66} elastic constants cross. At this pressure, the transverse acoustic waves in the basal plane, which are shown to be closely related to the symmetry breaking strain component that leads to the phase transition, become easier to excite than the ones with displacement along the c axis. It is found that this crossover pressure is an upper limit to the actual phase transition pressure. The average of the calculated equilibrium transition pressure and the crossover pressure is proposed as a good estimate for the actual transition pressure in cases where the transition is strongly kinetically hindered by an enthalpy barrier between the two phases. This occurs for SiC and GaN and is confirmed with literature data for AlN. For the remaining materials, all these pressures are close to each other. The trends of the elastic constants and sound velocities with the materials' Phillips scale ionicity are also reported.

DOI: 10.1103/PhysRevB.82.035201 PACS number(s): 61.50.Ks, 62.65.+k

I. INTRODUCTION

Most group-IV, III-V, and II-VI-semiconductors are well known to undergo a high-pressure phase transition from a tetrahedrally bonded phase to an octahedrally bonded phase. Most prior work has focused on determining the equilibrium transition pressure, at which the two phases have the same enthalpy. Recently, however, several studies have started to study the mechanism of transformation from one phase to the other. In particular, homogeneous transition paths have been proposed between wurtzite and rocksalt[1–3] and zincblende and rocksalt.[4–7] In such mechanisms, the transformation happens by a continuous deformation from one structure to the other by imposed strains. At each strain, the internal coordinates (i.e., atomic positions) are required to adjust to minimize the energy. For example, for the wurtzite to rocksalt transformation, the two strains correspond to a c/a reduction perpendicular to the basal plane and a strain in the basal plane along the $[10\bar{1}0]$ direction or any direction which is $\pm 60°$ or $\pm 120°$ from it, which we can call the b/a direction. On the experimental side, advanced diffraction techniques utilizing high brilliance synchrotron x-rays open up the opportunity to study crystal structures under high pressure in more detail.[8–11] Although the actual transition mechanism is likely to be more complex than a homogeneous transformation, as shown for example by molecular dynamics studies,[12] the homogeneous transformation path provides a useful simplified picture which may in reality happen locally in small regions and determine the nucleation event of the transition. Sarasamak *et al.*[3] studied the enthalpy landscapes in this space of strains driving the homogeneous transformation. Such enthalpy landscapes can be constructed at different hydrostatic pressures. By constructing such enthalpy landscapes, one can gain insight in the behavior of the system along various paths from one phase to the other within the strain coordinates. The local curvatures in different directions for example will tell us in which direction the system will initially most easily deform. The elastic constants are closely related to the local shape of this enthalpy landscape. In fact, they essentially determine the curvatures near the minima on this energy landscape. It is thus of interest to determine the elastic constants as function of pressure to better understand the initial stages of phase transition.

The elastic constants are also closely related to the sound velocities. Thus studying the sound velocities as function of pressure provides possibly an experimental way to determine the pressure dependence of the elastic constants. In fact, homogeneous strains are simply the long-wavelength limit of the acoustic phonon modes. The relation between sound waves in specific directions and the strains involved in the zincblende and wurtzite to rocksalt transition were previously pointed out by Prikhodko *et al.*[13]

Here, we study the elastic constants and sound velocities as function of direction and pressure in various wurzite crystals: SiC, GaN, InN, ZnO, and CdSe. Our choice of materials includes a IV-IV, two III-V, and two II-VI compounds. These

materials also have varied transition pressures. As will be seen, rather different behavior is obtained for different materials. Because we have systematically studied several materials, we can investigate the trend of the elastic constants and sound velocities with respect to the ionicity of material.

The paper is organized as follows. In Sec. II, we give the expressions for the sound velocities in different direction as function of the elastic constants. The calculation of elastic constants as function of pressure is also discussed. Essentially, they are obtained by calculating the total energy as function of a set of strains. Details of the computational method used to calculate the total energies from first principles are given in Sec. III. The results for the elastic constants and sound velocities in specific high-symmetry directions as function of pressure are presented in Sec. IV. In this section, the trend of the elastic constants and sound velocities with respect to the ionicity of material with also be presented. A summary of the main results is given in Sec. V.

II. THEORY

A. Sound velocities

The acoustic vibrational modes of a solid in the long-wavelength limit are obtained from the Christoffel equation,[14]

$$\rho\omega^2 u_i = M_{il}u_l, \tag{1}$$

where ρ is the mass density, ω the vibrational angular frequency, u_i the displacement amplitudes and summation convention is used for repeated Cartesian indices. The matrix M_{il} is given by

$$M_{il} = c_{ijkl}k_j k_k, \tag{2}$$

where c_{ijkl} is the elastic constant tensor elements, and k_j the wave vector components of the vibrational wave. Using Voigt notation, in the case of an hexagonal crystal (will be explained later), the M_{il} matrix reduces to

$$\begin{bmatrix} C_{11}k_x^2 + C_{66}k_y^2 + C_{44}k_z^2 & (C_{12}+C_{66})k_xk_y & (C_{13}+C_{44})k_xk_z \\ (C_{12}+C_{66})k_xk_y & C_{66}k_x^2 + C_{11}k_y^2 + C_{44}k_z^2 & (C_{13}+C_{44})k_yk_z \\ (C_{13}+C_{44})k_xk_z & (C_{13}+C_{44})k_yk_z & C_{44}(k_x^2+k_y^2) + C_{33}k_z^2 \end{bmatrix}. \tag{3}$$

For any direction the eigenvectors will be a quadratic function of $k=|\mathbf{k}|$ and hence $\omega=c_n(\hat{k})k$ with $c_n(\hat{k})$ the sound velocity for polarization n and direction $\hat{k}$. The results for hexagonal crystals were reported before by Rosen and Klimker.[15] For example, for $\mathbf{k}$ along [001], $k_x=k_y=0$ and $k_z=k$, the sound velocities become

$$c_{TA}([001]) = \sqrt{C_{44}/\rho}, \quad \text{with} \quad \text{twofold} \quad \text{degeneracy}$$

$$c_{LA}([001]) = \sqrt{C_{33}/\rho}, \tag{4}$$

where TA and LA stand for transverse and longitudinal acoustic.

Similarly, for any acoustic wave with wave vector in the basal plane, the sound velocities are given by the results for the [100] wave vector direction,

$$c_{LA}([100]) = \sqrt{C_{11}/\rho},$$

$$c_{TA[010]}([100]) = \sqrt{C_{66}/\rho},$$

$$c_{TA[001]}([100]) = \sqrt{C_{44}/\rho}, \tag{5}$$

where the first TA mode has displacements in-plane and the second one has displacements perpendicular to the basal plane. The results are independent of direction in the plane because we diagonalized a quadratic form representing an ellipsoid. Since this ellipsoid must have sixfold symmetry about the z axis, it must be an ellipsoid of revolution.

For a wave vector of the form $k_x=k\sin\theta$, $k_y=0$, $k_z=k\cos\theta$, the sound velocities are given by

$$\rho c_t(\theta)^2 = C_{66}\sin^2\theta + C_{44}\cos^2\theta,$$

$$\rho c_{\pm}(\theta) = \frac{C_{11}\sin^2\theta + C_{33}\cos^2\theta + C_{44}}{2} \pm \sqrt{\left[\frac{(C_{11}-C_{44})\sin^2\theta + (C_{44}-C_{33})\cos^2\theta}{2}\right]^2 + (C_{13}+C_{44})^2\cos^2\theta\sin^2\theta}. \tag{6}$$

TABLE I. Calculated equilibrium lattice constants of studied wurtzite semiconductors compared to experimental values.

		SiC	GaN	InN	ZnO	CdSe
a(Å)	Present	3.05	3.19	3.52	3.21	4.28
	Expt.	3.079[a]	3.19[b]	3.54[c]	3.26,[d] 3.253[a]	4.30,[e] 4.302[f]
c/a	Present	1.64	1.63	1.61	1.60	1.63
	Expt.	1.64[a]	1.627[b,g]	1.609[c]	1.60[a]	1.63[e,f]
u	Present	0.38	0.38	0.38	0.38	0.38
	Expt.	0.376[a]			0.382[a]	
V(Å^3)	Present	40.56	44.59	61.03	45.66	111.52

[a]XRD experiment by Schulz and Thiemann (Ref. 22).
[b]Synchrotron EDXD experiment by Xia *et al.* (Ref. 8).
[c]XRD experiment by Osamura *et al.* (Ref. 23).
[d]Synchrotron EDXD experiment by Desgreniers (Ref. 9).
[e]X-ray powder method by Hotje *et al.* (Ref. 24).
[f]XRD experiment by Sowa (Ref. 25).
[g]XAS experiment by Perlin *et al.* (Ref. 26).

This reduces to the in-plane limit for $\theta=\pi/2$ and along c limit for $\theta=0$.

As will be seen below, at zero pressure, we find for all wurtzite crystals studied here that $C_{44}<C_{66}$. Hence, the lowest TA sound velocity occurs for polarization along c and a wave vector in the plane or a wave vector along c and polarization in the plane. Obviously C_{11} and C_{33} corresponding to the longitudinal sound velocities are significantly higher.

B. Relation to strains and phase transition

To see the relation between specific sound waves to the wurtzite-to-rocksalt phase transitions, we analyze the strains related to the phase transitions and strains induced by related sound waves. A pure c/a strain can be written as

$$\begin{bmatrix} -\epsilon/2 & 0 & 0 \\ 0 & -\epsilon/2 & 0 \\ 0 & 0 & \epsilon \end{bmatrix}. \tag{7}$$

For $\epsilon<0$, it corresponds to a compression along c combined with an expansion in the plane in all directions such that the volume is preserved. This strain maintains the hexagonal symmetry of the crystal. As discussed, elsewhere, this transformation by itself could transform the wurtzite into the so-called HX-structure.[1,3] The latter differs from wurtzite by the fact that the layers become unbuckled or flat. At some critical value of this strain, the internal coordinate finds a minimum energy for $u=1/2$. Here, u is the conventional wurtzite internal parameters. The structure is fivefold coordinated from that point on.

The b/a distortion can be written as

$$\begin{bmatrix} -\epsilon & 0 & 0 \\ 0 & \epsilon & 0 \\ 0 & 0 & 0 \end{bmatrix}. \tag{8}$$

For $\epsilon>0$, it corresponds to a compression along the chosen **b** direction and a corresponding expansion perpendicular to it in the plane and no distortion along **c**. This is a pure in-plane shear strain and corresponds to the limit of a transverse sound wave at 45° from it. In fact, for a wave written as $u_y(x)=u_y^0\exp(ik_x x)$, the strain matrix has the form

$$\begin{bmatrix} 0 & \epsilon & 0 \\ \epsilon & 0 & 0 \\ 0 & 0 & 0 \end{bmatrix}, \tag{9}$$

which when diagonalized, gives a strain of the form of Eq. (8) with eigenvectors rotated 45° from the original axes in the plane. This means that the in-plane transverse acoustic sound waves at an angle 45° from the **b** directions correspond exactly to the symmetry breaking strain involved in the wurtzite to rocksalt transition, the strain we usually call the b/a strain. Thus the excitation of such sound waves could be viewed as the initial step in creating a b/a strain.

TABLE II. Bulk moduls B, its pressure derivative B' and elastic constants (in GPa) for wurtzite SiC (2H-SiC) compared with experimental data on 6H-SiC.

	B (GPa)	B'	C_{11}	C_{12}	C_{13}	C_{33}	C_{44}	C_{66}
Present	229	3.6	541	117	61	586	162	212
Expt.[a]	220		501	111	52	553	163	195

[a]Brillouin scattering experiment by Kamitani *et al.* (Ref. 27).

TABLE III. Bulk moduls B, its pressure derivative B' and elastic constants (in GPa) for wurtzite GaN compared with other calculations and experimental data.

	B (GPa)	B'	C_{11}	C_{12}	C_{13}	C_{33}	C_{44}	C_{66}
Present	207	4.2	367	135	98	409	98	116
Other[a]	207	4.5	346	148	105	389	76	99
Other[b]	202		367	135	103	405	95	116
Other[c]	201	4.3	366	139	98	403	97	
Expt.[d]	210		390	145	106	398	105	122
Expt.[e]	188	3.2						
Expt.[f]	245	4.0						
Expt.[g]	237	4.3						

[a]DFT(LDA) calculation by Kim *et al.* (Ref. 28).
[b]DFT(LDA) calculation by Wright (Ref. 16).
[c]DFT(LDA) calculation by Łepkowski *et al.* (Ref. 29).
[d]Brillouin scattering experiment by Polian *et al.* (Ref. 30).
[e]Synchrotron EDXD experiment by Xia *et al.* (Ref. 8).
[f]XAS experiment by Perlin *et al.* (Ref. 26).
[g]XRD experiment by Ueno *et al.* (Ref. 31).

The elastic constant defining the sound velocity for this type of acoustic sound waves is C_{66}. On the other hand, sound waves in the plane with displacement along the **c** axis or with wave vectors along **c** involve C_{44}. Now, because $C_{44}<C_{66}$, we can see that sound waves producing the b/a distortion are not the easiest to excite. For any finite wave vector, they require a bit higher energy. However, as we will see at some pressure the situation reverses and the C_{66} becomes the lower one. It is thus of interest to check whether the pressure where this crossing happens is in some ways related to the initiation of the phase transition.

III. COMPUTATIONAL METHOD

A. Elastic constant calculation

First, we briefly recall how to calculate elastic constants. The elastic energy (per unit volume) can be written as

$$U = \frac{1}{2}\epsilon_{ij}c_{ijkl}\epsilon_{kl}. \tag{10}$$

In Voigt notation, this becomes a matrix equation

$$U = \frac{1}{2}e_\lambda C_{\lambda\mu}e_\mu, \tag{11}$$

where $e_1=\epsilon_{xx}$, $e_2=\epsilon_{yy}$, $e_3=\epsilon_{zz}$, $e_4=2\epsilon_{yz}$, $e_5=2\epsilon_{zx}$, and $e_6=2\epsilon_{xy}$. The elastic constants follow a similar contraction of indices rule, e.g., $C_{12}=c_{xxyy}$, $C_{44}=C_{yzyz}$, etc. Since for a hexagonal material there are 5 independent elastic constants, we can choose 5 independent strains, calculate their elastic energy per unit volume and write it in terms of the appropriate combination of elastic constants. We will obtain 5 equations with 5 unknowns from which the elastic constants can be extracted. Following Wright *et al.*,[16] we can use the following strains and obtain the combination of elastic constants corresponding to each of them:

$$e = (\epsilon,\epsilon,0,0,0,0) \rightarrow U = (C_{11}+C_{12})\epsilon^2,$$

$$e = (\epsilon,\epsilon,-2\epsilon,0,0,0) \rightarrow U = (C_{11}+C_{12}-4C_{13}+2C_{33})\epsilon^2,$$

$$e = (0,0,\epsilon,0,0,0) \rightarrow U = \frac{1}{2}C_{33}\epsilon^2,$$

TABLE IV. Bulk moduls B, its pressure derivative B' and elastic constants (in GPa) for wurtzite InN compared with other calculations and experimental data.

	B (GPa)	B'	C_{11}	C_{12}	C_{13}	C_{33}	C_{44}	C_{66}
Present	151	4.8	232	115	96	239	52	59
Other[a]	147	3.4	220	120	91	249	36	50
Other[b]	141		223	115	92	224	48	54
Other[c]	146	3.9	229	120	95	234	49	
Expt.[d]	125	12.7						

[a]DFT(LDA) calculation by Kim *et al.* (Ref. 28).
[b]DFT(LDA) calculation by Wright (Ref. 16).
[c]DFT(LDA) calculation by Łepkowski *et al.* (Ref. 29).
[d]XRD experiment by Ueno *et al.* (Ref. 31).

TABLE V. Bulk moduls B, its pressure derivative B' and elastic constants (in GPa) for wurtzite ZnO compared with other calculations and experimental data.

	B (GPa)	B'	C_{11}	C_{12}	C_{13}	C_{33}	C_{44}	C_{66}
Present	162	4.0	227	133	118	232	40	47
Other[a]			217	117	121	225	50	50
Other[b]			231	111	104	183	72	60
Expt.[c]			206	118		211	44.3	44.6
Expt.[d]	181	4.0	209.7	121.1	105.1	210.9	42.47	44.3
Expt.[e]	206	4.0	207	117.7	106.1	209.5	44.8	44.65

[a]DFT(LDA) calculation by Gopal and Spaldin (Ref. 32); for C_{66} we used the value from $(C_{11}-C_{12})/2$.
[b]Atomistic simulation techniques based on the shell model calculation by Zaoui and Sekkal (Ref. 33).
[c]Brillouin scattering experiment Carlotti *et al.* (Ref. 34).
[d]B and B' from Synchrotron EDXD experiment by Decremps *et al.* (Ref. 10), C_{ij} from Ultrasound measurements by Bateman (Ref. 35).
[e]B and B' from Synchrotron EDXD experiment by Wu *et al.* (Ref. 11), C_{ij} from Kobiakov (Ref. 36).

$$e = (0,0,0,0,0,\epsilon) \rightarrow U = \frac{1}{4}(C_{11} - C_{12})\epsilon^2,$$

$$e = (0,0,0,\epsilon,\epsilon,0) \rightarrow U = C_{44}\epsilon^2. \quad (12)$$

Note that for the calculations under each of these strains the internal coordinates are allowed to relax. Also, note that in the latter two cases, the hexagonal symmetry is broken by the distortion. Now, we want to calculate all these elastic constants as functions of pressure. We first determine the undistorted structure total energy as function of volume, and from $p=-\partial E/\partial V$ determine the pressure corresponding to each volume. In practice, we fit the Murnaghan equation of state to the $E(V)$ results and invert it to obtain volume as function of pressure.

At each pressure, and the corresponding volume, we apply the strains defined in Eq. (12) and, thus, obtain the elastic energy and consequently the pressure dependent elastic constants. Although some of these strains are volume conserving, e.g., the second and last two, the others are not and contain a hydrostatic component. Still, we use the volume at pressure p before applying the distortion in defining the energy per unit volume in those cases, which is sufficient because we only consider linear elasticity theory. In other words, we make a quasiharmonic approximation.

B. Computational details

To obtain all total energies required for the calculation of the elastic constants we use the Kohn-Sham density functional theory[17,18] in the local density approximation with the Perdew-Zunger parametrization of exchange and correlation.[19] The total energies are calculated using the full-potential linearized muffin-tin orbital method as described by Methfessel and van Schilfgaarde.[20] Well converged double basis sets are utilized and the Brillouin zone integrations are done using a $4\times4\times4$ Monkhorst-Pack sampling set.[21]

IV. RESULTS

A. Elastic constants and sound velocities at zero pressure

First, we give our results obtained for the equilibrium properties of the materials investigated here compared to experimental results. Table I shows the wurtzite lattice constants a, c/a, internal parameter u and the volume of the unit cell. Excellent agreement is obtained in all cases.

Tables II–VI give our results for the elastic constants at zero pressure compared with literature values. Overall, good agreement is obtained both with experimental and calculated values by others. For SiC, the wurtzite phase, which is usually called 2H-SiC is difficult to grow and, therefore, no experimental data on elastic constants of 2H-SiC are avail-

TABLE VI. Bulk moduls B, its pressure derivative B' and elastic constants (in GPa) for wurtzite CdSe compared with other calculations and experimental data.

	B (GPa)	B'	C_{11}	C_{12}	C_{13}	C_{33}	C_{44}	C_{66}
Present	60	4.6	80	47	40	92	15	17
Expt.[a]			74.9	46.09	39.36	84.51	13.15	14.40
Expt.[b]	53.3	4.0	74.1	45.2	39.3	83.6	13.17	14.45

[a]Ultrasound measurements by Cline *et al.* (Ref. 37).
[b]B and B' from XRD experiment by Sowa (Ref. 25), C_{ij} from resonance measurement by Berlincourt *et al.* (Ref. 38).

TABLE VII. The second-order polynomials describing the pressure dependence of selected elastic constants for SiC, GaN, InN, ZnO, and CdSe. The polynomials were obtained from a fit to the calculated results at discrete pressures. The pressure, P, is in GPa and the ranges used for the fit are shown in the last column.

	Elastic constant (GPa)	P range (GPa)
SiC	$C_{11}=542+4.79P-0.0140P^2$	0–150
	$C_{33}=586+8.02P-0.0262P^2$	
	$C_{44}=163+0.91P-0.0015P^2$	
	$C_{66}=213+0.83P-0.0038P^2$	
GaN	$C_{11}=369+3.74P-0.0135P^2$	0–100
	$C_{33}=405+4.54P-0.0083P^2$	
	$C_{44}=98+0.58P-0.0023P^2$	
	$C_{66}=117+0.48P-0.0052P^2$	
InN	$C_{11}=232+3.86P-0.017P^2$	0–40
	$C_{33}=240+4.72P-0.036P^2$	
	$C_{44}=52+0.24P-0.001P^2$	
	$C_{66}=58-0.08P-0.005P^2$	
ZnO	$C_{11}=227+1.62P+0.073P^2$	0–16
	$C_{33}=232+1.16P+0.165P^2$	
	$C_{44}=40+0.03P-0.005P^2$	
	$C_{66}=47-0.86P+0.006P^2$	
CdSe	$C_{11}=81+3.53P-0.075P^2$	0–10
	$C_{33}=91+5.49P-0.197P^2$	
	$C_{44}=15+0.05P-0.026P^2$	
	$C_{66}=17+0.11P-0.111P^2$	

able. However, one finds that the elastic constants for 4H and 6H SiC, two slightly different polytypes, are very close to each other. We thus compare with the values for 6H.

The sound velocities at zero pressure extracted from these at zero pressure are given in Tables VIII for wave vector directions along [001] and [100]. As discussed above, the sound velocities for wave vectors in the plane are independent of the direction angle in the plane. For wave vectors that are intermediate between in-plane and perpendicular to the basal plane, the sound velocities have a well defined angular dependence given in Eq. (6).

B. Pressure dependent elastic constants and sound velocities

In Figs. 1 and 2, we show the pressure dependence of the elastic constants and sound velocities, respectively. The dots show the first principles results for the given pressures. The lines are the second-order polynomial fit to the results. The fitting results (quadratic equations) for the elastic constants are shown in Table VII. We can see quite different behaviors depending on the material and the elastic constants considered. The compressional moduli, C_{11} and C_{33} are increasing with pressure but for most materials we see that C_{33} curves downward at higher pressures. The exception is ZnO, where it curves upward. For SiC and GaN, the shear type elastic constant C_{66} initially increases but goes through a maximum and then bends down. For InN, ZnO, and CdSe, it monotonically decreases with increasing pressure starting from zero pressure. In ZnO, it slightly curves upward instead of downward. The C_{44} changes from increasing with pressure in SiC, GaN, and InN, to staying almost constant in ZnO and decreasing in CdSe. Since the sound velocities are directly derived from these elastic constants, similar behavior is also observed. Their behavior is, however, slightly different because the mass density involved in the sound velocity also changes as a function of pressure. To the best of our knowledge, no measurements of the sound velocities or elastic constants as function of pressure are available for these materials. Our calculations predict and interesting variety of behaviors, which would be beneficial to verify experimentally. The elastic constants as function of pressure were previously calculated using DFT by Łepkowski *et al.*[29] for GaN and InN. They extracted the linear and quadratic pressure coefficients. Their results for the two materials are comparable to ours (as shown in Fig. 1), but we considered a larger pressure range. For ZnO, the elastic constants as function of pressure were previously calculated by Zaoui and Sekkal[33] but using only pair potential shell model level of calculations. For CdSe, the elastic constants as a function of pressure were previously studied for only the zincblende phase by Deligoz *et al.*[41]

C. Relation to phase transition

As discussed in the introduction, it is of interest to consider the pressure where C_{44} crosses with C_{66}. Above this pressure, transverse sound waves in the basal plane should become easier to excite than sound waves related to c/a strains. The transverse sound waves are closely related to the symmetry breaking b/a strain leading to the phase transition, while the sound waves related to c/a strains preserve the hexagonal symmetry. In order to initiate the phase transition, it might seem important to break the symmetry.

We thus consider the pressures where these two shear elastic constants cross, or equivalently where the sound velocities cross. The values are summarized in Table IX along with the equilibrium phase transition pressure (the pressure where the calculated enthalpies of the rocksalt and wurtzite phases are equal) and the experimentally observed phase transition pressures. We estimate the uncertainty on these crossover pressures to be of the order a few GPa.

We can see that for SiC, GaN, and CdSe the cross-over pressure is higher than the actual transition pressure, while the equilibrium transition pressure is lower than the experimental value. The latter has been previously attributed to the existence of a barrier between the two phases at the transition pressure. It can be considered a kinetic effect. For InN, our calculated equilibrium transition pressure is in good agreement with the experimental value while the crossover pressure is higher. Note that, generally the InN crystal quality is quite poor so the measurement of this particular material might contain a sizable error bar. For ZnO, the calculated crossover pressure is slightly higher than the calculated equilibrium transition pressure. The observed experimental transition pressures of 9.1–10.5 GPa exceeds both of these values but by only ≈ 1 GPa, which is well within the computational error bar.

TABLE VIII. Sound velocities (in km/s) at zero pressure for SiC, GaN, InN, ZnO, and CdSe calculated from the elastic constants. $\hat{k}$ is the wave vector and $\boldsymbol{n}$ is the polarization. The Phillips ionicity parameters (f_i) are also listed.

		$\hat{k}\rightarrow$	[100]			[001]	
	f_i	$\boldsymbol{n}\rightarrow$	[100]	[001]	[010]	[001]	[100]
SiC	0.177	Present	12.8	7.0	8.0	13.4	7.0
		Other[a]	12.5	7.1	7.8	13.1	7.1
		Expt.[b]				12.21	7.69
		Expt.[c]				13.27	7.24
GaN	0.500	Present	7.67	3.96	4.32	8.10	3.96
		Other[d]	8.0	4.1	6.3	8.0	4.1
InN	0.578	Present	5.76	2.73	2.89	5.84	2.73
		Other[d]	5.3	1.2	2.5	5.2	1.2
ZnO	0.616	Present	6.23	2.61	2.83	6.30	2.61
		Other[e]	6.08	2.92	2.92	6.19	2.92
		Expt.[f]	6.08	2.73	2.79	6.10	2.73
CdSe	0.699	Present	3.76	1.62	1.71	4.02	1.62
		Expt.[g]	3.63	1.52	1.59	3.86	1.52

[a]Calculated from elastic constants by Kamitani *et al.* (Ref. 27).
[b]Ultrasound measurements by Schreiber *et al.* (Ref. 39).
[c]Raman measurements on various polytypes, Feldman *et al.* (Ref. 40).
[d]Calculated from elastic constants by Wright *et al.* (Ref. 16).
[e]Calculated from elastic constants by Gopal and Spaldin (Ref. 32).
[f]Ultrasound measurements by Bateman (Ref. 35).
[g]Ultrasound measurements by Cline *et al.* (Ref. 37).

As discussed before by Limpijumnong and Jungthawan,[42] for more ionic or softer tetrahedral semiconductors, the calculated transition pressures are close to the experimental ones, while for the stiffer ones, the calculated equilibrium transition pressures are significantly underestimated. The underestimation of the calculated transition pressure was attributed to the kinetic barrier in the actual transition. Here, we observe some relationship between the crossover pressure and the transition pressure. We find that the crossover pressure might serve as an upper limit of the transition pressure. In addition, we propose that in combination with the calculated equilibrium transition pressure it can be used to improve the prediction of the actual transition pressure, as will be described later. This observation is especially useful for the stiffer materials, for e.g., SiC and GaN in our present study, where the calculated transition pressure is significantly underestimated.

Above the crossover pressure, the transverse sound waves associated with C_{66} turn easier to excite than sound waves associated with C_{44}. However, even before the C_{66} and C_{44} cross, one may expect that as they approach each other it already become probable to excite the transverse acoustic waves at finite temperature and ultimately initiate the transition. Note that in this model, we consider the excitation of such modes as the triggering effect. Once the system starts exhibiting a strain of this type, the c/a distortion follows it through the anharmonic interactions between these two types of modes. This then leads the system toward the barrier transition point which separates the wurtzite from the rocksalt valley as can be seen from the energy landscapes given in Sarasamak *et al.*[3] Note that the excitation energy of the phonon with the wavelength of about 1 nm can be estimated from $\hbar\omega=\hbar vk\approx 10-20$ meV, which is comparable to the thermal energy at room temperature. This means that within a nucleation region of about 1 nm the homogeneous transformation might be triggered already at room temperature and serves as a nucleus of the new phase.

From Table IX, it is clear that the calculated equilibrium transition pressure p_t generally underestimates the experimentally observed pressure p_u by about as much percentage wise as the crossover pressure overestimates it. Therefore, we propose that a good and simple approximation to the experimental pressure would be $(p_t+p_c)/2$. Our calculated values of $(p_t+p_c)/2$ are tabulated in Table IX and are very close the experimental values for SiC and GaN. As a further test that this gives a useful estimate in particular for cases where there is evidence of a significant transition kinetic barrier, we consider AlN. Based, on the data of Łepkowski *et al.*[29] for the pressure-dependent elastic constants, we obtain the crossover pressure to be 39.6 GPa. The calculated equilibrium transition pressure by Serrano *et al.*[43] is 9.2 GPa. This gives as estimate for the actual transition pressure $(p_t+p_c)/2=24.4$ GPa. The experimental value by Ueno *et al.*[44] is 22.9 GPa.

Note that the correlation found here between the sound wave excitations of a particular symmetry and the transition pressures is suggestive but not a complete proof of their roles in the actual transition processes. The actual transition re-

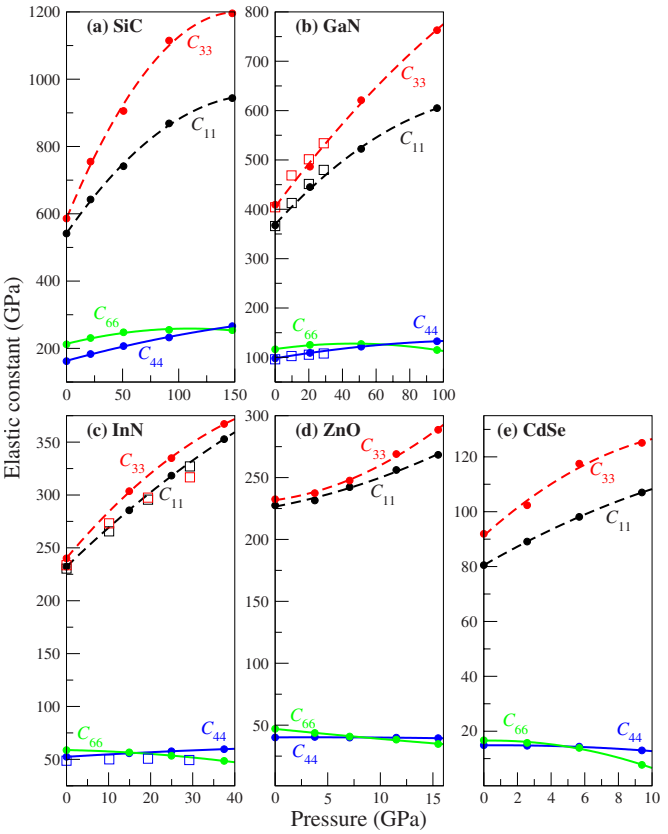

FIG. 1. (Color online) Calculated pressure dependence of the elastic constants in (a) SiC, (b) GaN, (c) InN, (d) ZnO, and (e) CdSe. In (b) and (c), the square symbols show the calculated results by Łepkowski *et al.* (Ref. 29).

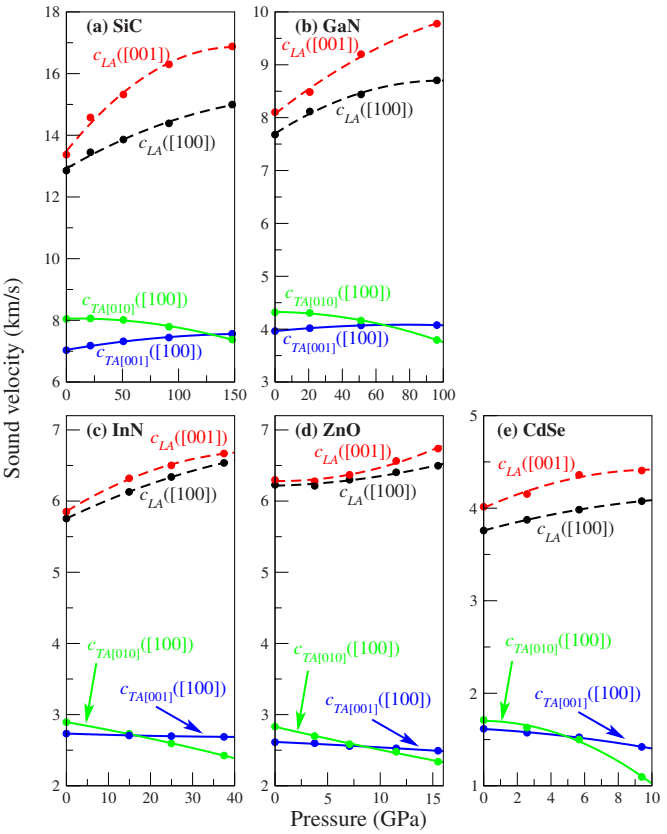

FIG. 2. (Color online) Calculated pressure dependence of the sound velocities in (a) SiC, (b) GaN, (c) InN, (d) ZnO, and (e) CdSe.

quires the occurrence of both in-plane and perpendicular to the plane types of strain to reach the transition barrier. The transition barrier height[42] and the overall enthalpy landscape[3] therefore play a significant role in the phase transformation process.

D. Trends with ionicity

Because we have systematically calculated several wurtzite crystals, i.e., SiC, GaN, InN, ZnO, and CdSe, that spanned a wide range of ionicity, we can study the trend of the elastic constants and sound velocities with the material's ionicity. To quantify the ionicity of these materials, we choose to use Phillips' ionic scale[45] (f_i) which has the range between 0 (completely covalent) and 1 (completely ionic). This scale is based on optical properties of the semiconductors and has been shown in the past to be related to the preference for octahedral and tetrahedral bonding and the transition pressures.[46,47] The values of f_i for the materials studied are listed in Table VIII. In Fig. 3(a), we plotted the elastic constants as a function of f_i at zero pressure. We can see that all four elastic constants monotonically decrease as f_i increases. The same holds true at finite pressures. For the sound velocity, the general trend also follows that of the elastic constant because the sound velocity is proportional to the square root of the corresponding elastic constant as shown in Eq. (4) and (5). In Fig. 3(b), the sound velocities are shown as a function of f_i. We note that in both the LA sound velocities and compressional elastic constants, InN dips a bit below the trend lines. This may be indicative of the

TABLE IX. Crossover pressure p_c where $C_{44}=C_{66}$, calculated equilibrium phase transition pressure p_t (taken from Ref. 3, except for AlN) and experimental transition pressures p_u for wurtzite-to-rocksalt transition, all in GPa, for SiC, GaN, AlN, InN, ZnO, and CdSe.

	p_c	p_t	$(p_t+p_c)/2$	p_u
SiC	131.1	64.9	98.0	100[a]
GaN	65.5	44.1	54.8	52.2[b]
AlN	39.6[c]	9.2[d]	24.4	22.9[e]
InN	15.7	12.2	13.9	12.1[b]
ZnO	8.8	8.2	8.4	9.1[f], 10.5[g]
CdSe	5.2	2.2	3.7	4.0[h]

[a]XRD experiment by Yoshida *et al.* (Ref. 50).
[b]XRD experiment by Ueno *et al.* (Ref. 31).
[c]Calculated here from data of Łepkowski *et al.* (Ref. 29).
[d]From Serrano *et al.* (Ref. 43).
[e]From Ueno *et al.* (Ref. 44).
[f]Synchrotron XRD experiment by Desgreniers (Ref. 9).
[g]Synchrotron EDXD experiment by Kumar *et al.* (Ref. 51).
[h]Synchrotron XRD experiment by Wang *et al.* (Ref. 52).

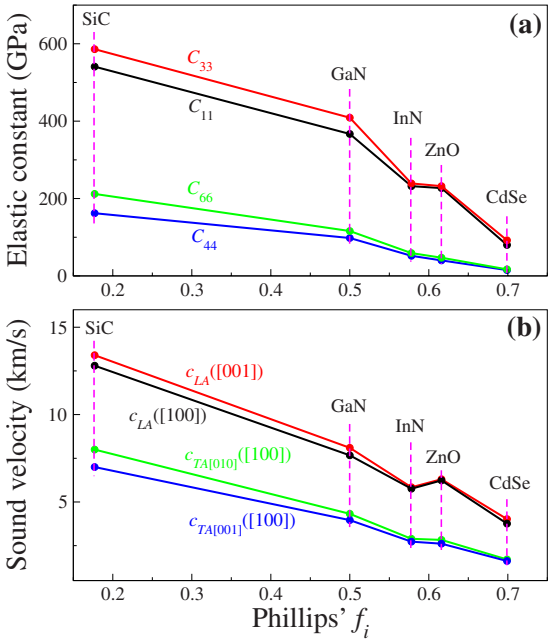

FIG. 3. (Color online) Calculated (a) elastic constants and (b) sound velocities as a function of ionicity (Phillips' scale) at zero pressure ($P=0$ GPa).

fact that the ionicity of InN is underestimated by the Phillips scale. InN has a larger ionicity in the Garcia scale.[48] The ionicities of the III-nitrides were discussed in Ref. 49

V. CONCLUSIONS

We presented the calculated elastic constants and sound velocities in wurtzite SiC, GaN, InN, ZnO, and CdSe as functions of pressure. We found interesting nonlinear behavior of the elastic constants and sound velocities with pressure that is quite different in the different materials. We also showed that the elastic constants are lower in materials with higher ionicity. Generally, the sound velocities follow the same trend as the elastic constants, i.e., lower in materials with higher ionicity. The pressure at which the C_{44} and C_{66} shear elastic constants cross are investigated. When C_{66} becomes lower, it should be easier to excite the symmetry breaking strain mode related to the wurtzite-to-rocksalt phase transition. We found that the crossover pressure is generally higher than the experimental transition pressure and explained it by the fact that finite temperature fluctuations make it possible to excite the required modes even before the two sound velocities cross. We proposed the average of the crossover and calculated equilibrium transition pressures to be a good estimate for the experimental transition pressure in cases where there is a significant transition enthalpy barrier. The results suggest that the in-plane transverse sound waves could play a significant role in triggering the phase transition. Of course, the details near the transition point, the height of the barrier, and the coupling of the in and out of plane acoustic modes, which are both required to reach the transition point, are also important for the transition to take place.

ACKNOWLEDGMENTS

This work was supported by Thailand Research Fund (Grant No. RTA5280009) and AOARD/AFOSR (Contract No. FA2386-09-1-4106).

[1] S. Limpijumnong and W. R. L. Lambrecht, Phys. Rev. Lett. **86**, 91 (2001a).
[2] S. Limpijumnong and W. R. L. Lambrecht, Phys. Rev. B **63**, 104103 (2001b).
[3] K. Sarasamak, A. J. Kulkarni, M. Zhou, and S. Limpijumnong, Phys. Rev. B **77**, 024104 (2008).
[4] M. Catti, Phys. Rev. Lett. **87**, 035504 (2001).
[5] M. S. Miao, M. Prikhodko, and W. R. L. Lambrecht, Phys. Rev. Lett. **88**, 189601 (2002).
[6] M. S. Miao, M. Prikhodko, and W. R. L. Lambrecht, Phys. Rev. B **66**, 064107 (2002).
[7] M. S. Miao and W. R. L. Lambrecht, Phys. Rev. Lett. **94**, 225501 (2005).
[8] H. Xia, Q. Xia, and A. L. Ruoff, Phys. Rev. B **47**, 12925 (1993).
[9] S. Desgreniers, Phys. Rev. B **58**, 14102 (1998).
[10] F. Decremps, F. Datchi, A. M. Saitta, A. Polian, S. Pascarelli, A. Di Cicco, J. P. Itié, and F. Baudelet, Phys. Rev. B **68**, 104101 (2003).
[11] X. Wu, Z. Wu, L. Guo, C. Liu, J. Liu, X. Li, and H. Xu, Solid State Commun. **135**, 780 (2005).
[12] S. E. Boulfelfel, D. Zahn, Y. Grin, and S. Leoni, Phys. Rev. Lett. **99**, 125505 (2007).
[13] M. Prikhodko, M. S. Miao, and W. R. L. Lambrecht, Phys. Rev. B **66**, 125201 (2002).
[14] L. D. Landau and E. M. Lifschitz, *Theory of Elasticity, Course of Theoretical Physics* (Pergamon Press, New York, 1980), Chap. 3, Vol. 7.
[15] M. Rosen and H. Klimker, Phys. Rev. B **1**, 3748 (1970).
[16] A. F. Wright, J. Appl. Phys. **82**, 2833 (1997).
[17] P. Hohenberg and W. Kohn, Phys. Rev. **136**, B864 (1964).
[18] W. Kohn and L. J. Sham, Phys. Rev. **140**, A1133 (1965).
[19] J. P. Perdew and A. Zunger, Phys. Rev. B **23**, 5048 (1981).
[20] M. Methfessel, M. van Schilfgaarde, and R. A. Casali, in *Electronic Structure and Physical Properties of Solids. The Uses of the LMTO Method, Lecture Notes in Physics*, edited by H. Dreyssé (Springer Verlag, Berlin, 2000), Vol. 535, p. 114.
[21] H. J. Monkhorst and J. D. Pack, Phys. Rev. B **13**, 5188 (1976).
[22] H. Schulz and K. H. Thiemann, Solid State Commun. **32**, 783 (1979).
[23] K. Osamura, S. Naka, and Y. Murakami, J. Appl. Phys. **46**, 3432 (1975).
[24] U. Hotje, C. Rose, and M. Binnewies, Solid State Sci. **5**, 1259 (2003).
[25] H. Sowa, Solid State Sci. **7**, 1384 (2005).
[26] P. Perlin, C. Jauberthie-Carillon, J. P. Itie, A. San Miguel, I. Grzegory, and A. Polian, Phys. Rev. B **45**, 83 (1992).

[27] K. Kamitani, M. Grimsditch, J. C. Nipko, C.-K. Loong, M. Okada, and I. Kimura, J. Appl. Phys. **82**, 3152 (1997).
[28] K. Kim, W. R. L. Lambrecht, and B. Segall, Phys. Rev. B **56**, 7018 (1997).
[29] S. P. Łepkowski, J. A. Majewski, and G. Jurczak, Phys. Rev. B **72**, 245201 (2005).
[30] A. Polian, M. Grimsditch, and I. Grzegory, J. Appl. Phys. **79**, 3343 (1996).
[31] M. Ueno, M. Yoshida, A. Onodera, O. Shimomura, and K. Takemura, Phys. Rev. B **49**, 14 (1994).
[32] P. Gopal and N. A. Spaldin, J. Electron. Mater. **35**, 538 (2006).
[33] A. Zaoui and W. Sekkal, Phys. Rev. B **66**, 174106 (2002).
[34] G. Carlotti, D. Fioretto, G. Socino, and E. Verona, J. Phys.: Condens. Matter **7**, 9147 (1995).
[35] T. B. Bateman, J. Appl. Phys. **33**, 3309 (1962).
[36] J. B. Kobiakov, Solid State Commun. **35**, 305 (1980).
[37] C. F. Cline, H. L. Dunegan, and G. W. Henderson, J. Appl. Phys. **38**, 1944 (1967).
[38] D. Berlincourt, H. Jaffe, and L. R. Shiozawa, Phys. Rev. **129**, 1009 (1963).
[39] E. Schreiber and N. Soga, J. Am. Ceram. Soc. **49**, 342 (2006).
[40] D. W. Feldman, J. H. Parker, W. J. Choyke, and L. Patrick, Phys. Rev. **173**, 787 (1968).
[41] E. Deligoz, K. Colakoglu, and Y. Ciftci, Physica B **373**, 124 (2006).
[42] S. Limpijumnong and S. Jungthawan, Phys. Rev. B **70**, 054104 (2004).
[43] J. Serrano, A. Rubio, E. Hernández, A. Munoz, and A. Mujica, Phys. Rev. B **62**, 16612 (2000).
[44] M. Ueno, A. Onodera, O. Shimomura, and K. Takemura, Phys. Rev. B **45**, 10123 (1992).
[45] J. C. Phillips, Rev. Mod. Phys. **42**, 317 (1970).
[46] J. R. Chelikowsky and J. K. Burdett, Phys. Rev. Lett. **56**, 961 (1986).
[47] N. E. Christensen, S. Satpathy, and Z. Pawlowska, Phys. Rev. B **36**, 1032 (1987).
[48] A. García and M. L. Cohen, Phys. Rev. B **47**, 4215 (1993).
[49] W. R. L. Lambrecht, in *Gallium Nitride (GaN) I, Semiconductors and Semimetals*, edited by J. I. Pankove and T. D. Moustakas (Academic Press, San Diego, 1998), Vol. 50.
[50] M. Yoshida, A. Onodera, M. Ueno, K. Takemura, and O. Shimomura, Phys. Rev. B **48**, 10587 (1993).
[51] R. S. Kumar, A. L. Cornelius, and M. F. Nicol, Curr. Appl. Phys. **7**, 135 (2007).
[52] Z. Wang, K. Finkelstein, C. Ma, and Z. L. Wang, Appl. Phys. Lett. **90**, 113115 (2007).